Electronic Supplementary Material (ESI) for Journal of Materials Chemistry A.
This journal is © The Royal Society of Chemistry 2024

Supplementary Information

Balancing triple conductivity of zinc-doped cathode for proton-conducting solid oxide fuel cells

Xiangbo Deng, [a] Mingming Zhang, [a] Min Fu, [a] Qian Wang,[b] and YuXuan Zhu[b] and Zetian Tao*[a]

[a] School of Resources, Environment and Safety Engineering, University of South China, Hengyang, Hunan Province, 421001, China

b. School of Chemistry and Chemical Engineering, University of South China, Hengyang, Hunan Province, 421001, China.

* Corresponding author.

Email address: newton@mail.ustc.edu.cn and taozetian@usc.edu.cn (Z. Tao).

1.Experimental Sections

$BaCe_{0.36-x}Fe_{0.64}Zn_xO_{3-\delta}$ (x = 0.05, 0.1, and 0.15), denoted as BCFZ05, BCFZ10, and BCFZ15 respectively, along with BCF36, BZCYY and NiO-BZCYY materials, were synthesized using a standard sol-gel method.[1] X-ray diffraction (XRD) analysis, conducted with a scanning 2θ angle range of 20°-80° using the Bruker D8 Advance instrument, was employed to assess the phase purity and composition of BCFZ05, BCFZ10, and BCFZ15, followed by Rietveld refinement using GSAS2 software. Furthermore, X-ray photoelectron spectroscopy (XPS) was utilized, employing the Thermo Scientific K-Alpha instrument, to characterize the chemical states of BCFZ05, BCFZ10, and BCFZ15. Microstructural features of the BCFZ series materials were examined using scanning electron microscopy (SEM, Nova NanoSEM 450). Additionally, the crystal structure and elemental distribution of the synthesized BCFZ10 were analyzed using high-resolution transmission electron microscopy (HR-TEM, JEM-2100F, JEOL, Japan). Proton uptake capability was assessed by subjecting the BCF36 and BCFZ10 samples to pre-treatment in 3% humid air at 200°C for 24 hours, followed by heating from 30°C to 800°C at a rate of 10°C/min. Mass loss ratio during the heating process was recorded using a thermos gravimetric analyzer (TGA, STA 449 C, Netzsch).

BCZYY is widely employed as an electrolyte in H-SOFCs due to its excellent stability, sintering activity, and proton conductivity. Single cells were fabricated using the NiO-

BZCYY/BZCYY/ $BaCe_{0.36-x}Fe_{0.64}Zn_xO_{3-\delta}$ composite via a process involving molding, co-sintering, screen printing, and microwave treatment at 900°C for 30 minutes. The single cell was fabricated using a process involving molding, co-sintering, screen printing, and microwave treatment at 900°C for 30 minutes, employing the NiO-BZCYY/BZCYY/BaCe0.36-xFe0.64ZnxO3-δ composite material. Specifically, the half-cell was prepared via dry pressing. Initially, a mixture of NiO, BZCYY, and corn starch in a weight ratio of 60%:40%:20% was pre-pressed to form the substrate. Subsequently, the anode functional layer and BZCYY electrolyte powder were sequentially pressed onto this substrate. The assembly was then sintered at 1350°C for 5 hours. The cathode slurry, obtained by grinding cathode powders and mixing them with terpineol for 2 hours, was applied via screen printing onto the electrolyte layer. Finally, the single cell configuration, NiO-BZCYY/BZCYY/BCFZ, was achieved by co-firing at 1000°C for 3 hours. It is noteworthy that microwave sintering of the cathode significantly reduces sintering time and temperature compared to conventional muffle furnace sintering, while preserving the cathode's original microstructure.[2] In single-cell testing, wet hydrogen gas with 3% water content (flow rate controlled at 25 mL min^{-1}) was used as the fuel gas, while oxygen was sourced from ambient air. The electrochemical performance of the single cell from 550°C to 700°C was recorded using an electrochemical workstation (Squidstat Plus), with the frequency range set from 1 MHz to 0.1 Hz for EIS testing. The electrical conductivity relaxation (ECR) technique was conducted using a four-probe method to test the electrical conductivity of dense ceramic rods of BCFZ05, BCFZ10, and BCFZ15 (sintered at 1250°C for 5 hours). It was used to monitor the time required to reach equilibrium after switching from dry air to gas with an oxygen-to-nitrogen ratio of 1:1, and the testing curves were fitted to observe detailed oxygen diffusion processes.

Theoretical calculations were conducted using density functional theory (DFT) within the Vienna Ab initio simulation package (VASP) 5, employing the projector-augmented-wave (PAW) method. The impact of Zn doping on electronic states and subsequent outcomes were assessed, focusing on factors such as oxygen vacancy formation energy, hydration ability, and proton migrations. Energy and force convergence criteria were set at 10^{-5} eV and 0.02 eV $Å^{-1}$, respectively. A kinetic energy cutoff of 400 eV for the plane wave basis set and a 4 × 4 × 4 gamma center grid for the K-point mesh were employed. Bulk structure optimization utilized 2 × 2 × 2 super cells for both BFZO and BFO. The spin-polarization method with generalized gradient approximation (GGA) and Perdew-Burke-Ernzerhof (PBE) exchange-correlation functional were applied for in-depth exploration of BFZO and BFO. Additionally, the climbing image nudged elastic band (CI-NEB) method was utilized to analyze proton migration reaction barriers.

2. Supplementary Figures

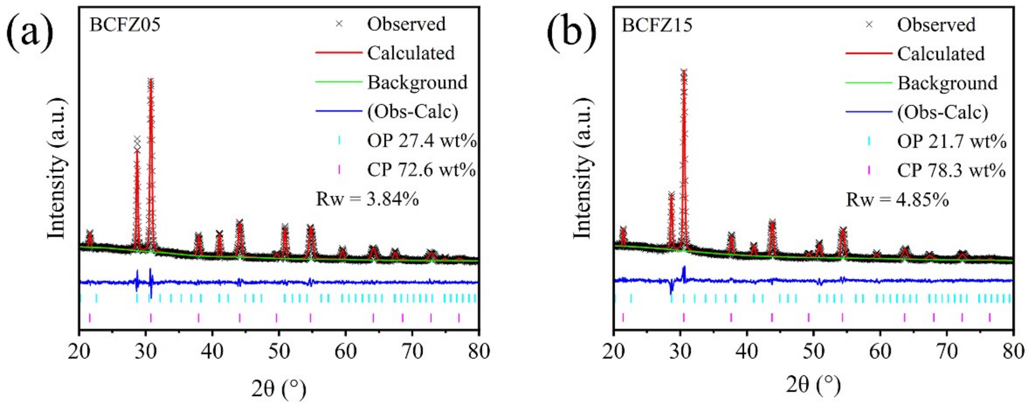

Fig. S1 Refined XRD patterns of (a) BCFZ05 and (b) BCFZ15 sample.

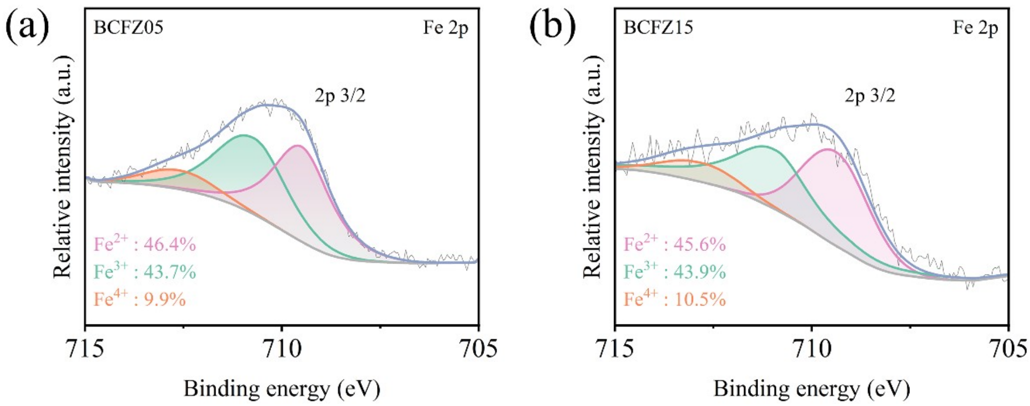

Fig. S2 Fe 2p XPS spectra of (a) BCFZ05 and (b) BCFZ15 samples.

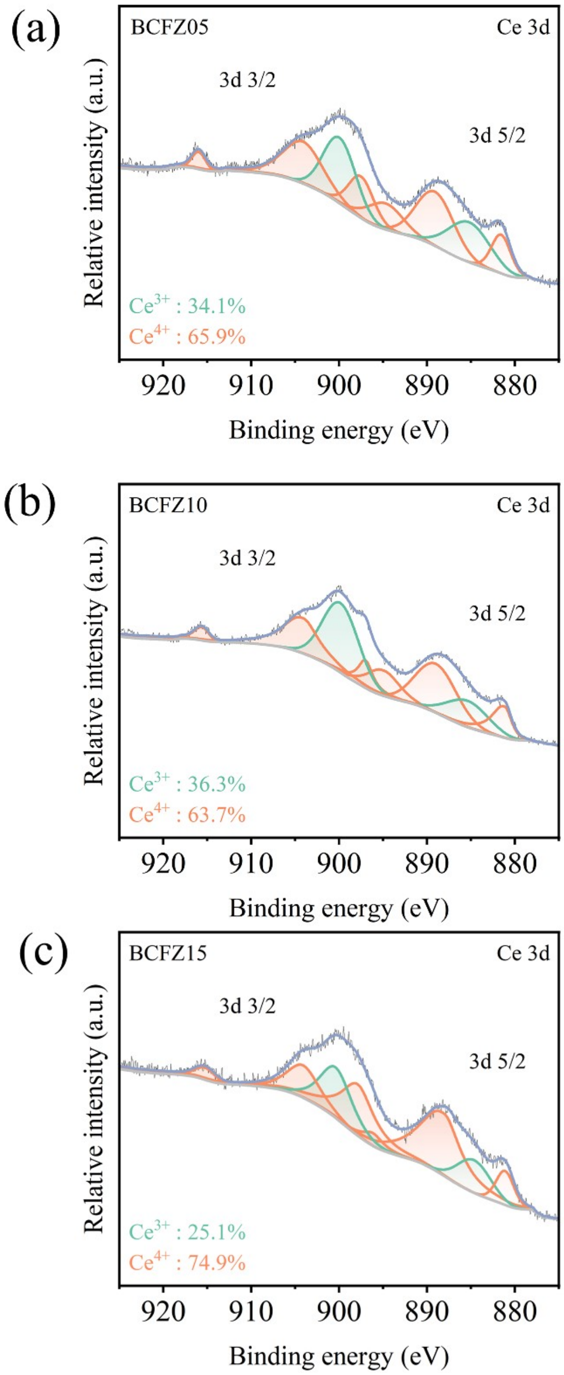

Fig. S3 Ce 3d XPS spectra of (a) BCFZ05, (b) BCFZ10 and (c) BCFZ15 samples.

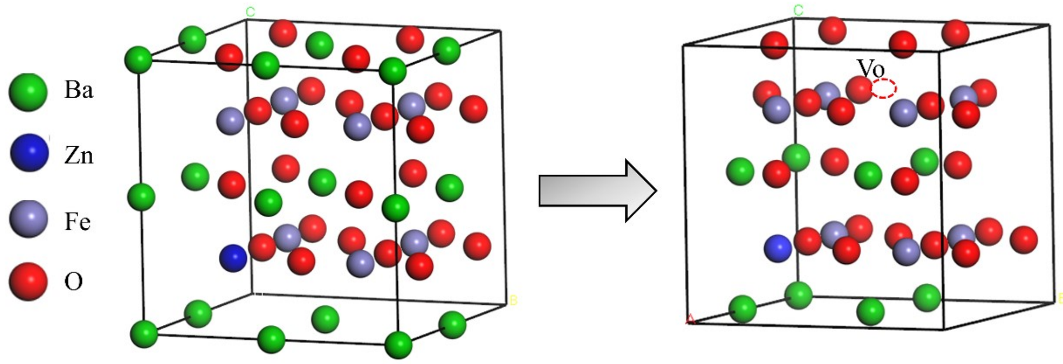

Fig. S4 The oxygen with red dashed circle stands for the position where oxygen vacancies (Vo) are created.

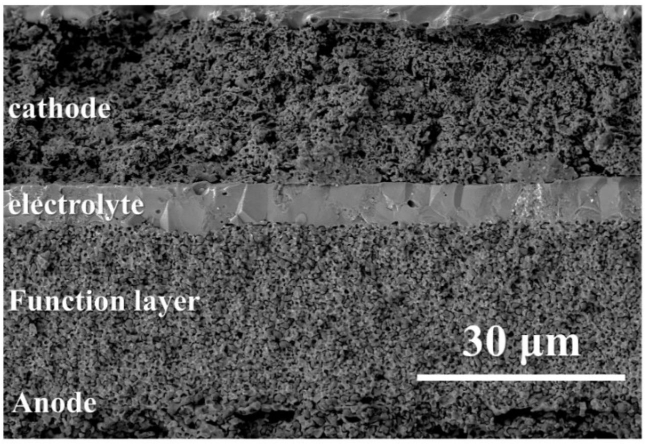

Fig. S5 Cross-sectional SEM image of the anode-supported single cell with BCFZ10 cathode.

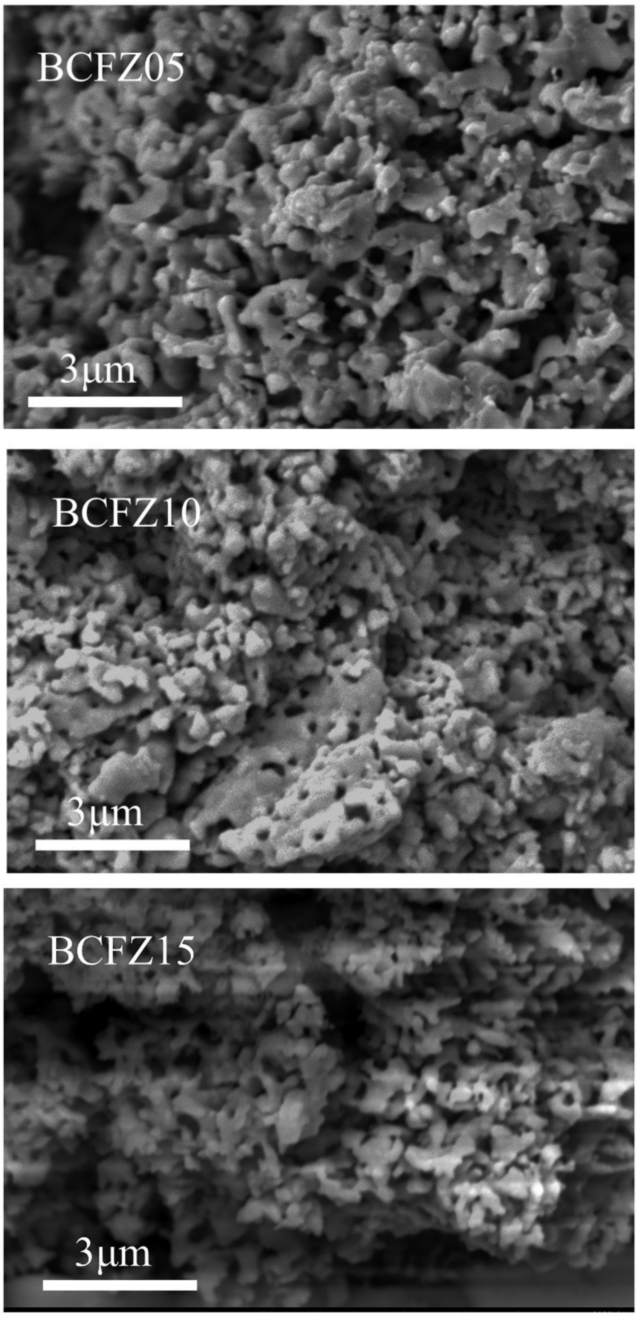

Fig. S6 SEM images of BCFZ05, BCFZ10 and BCFZ15 cathode samples.

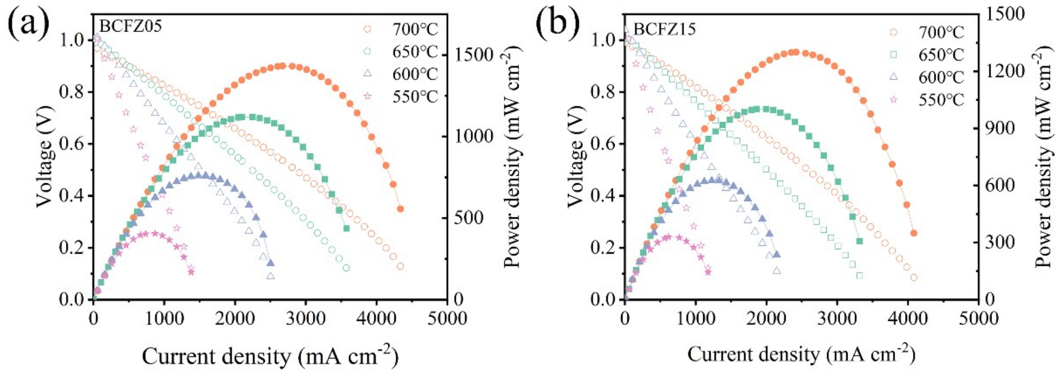

Fig. S7 *I-V* and *I-P* curves of anode-supported single cells with (a) BCFZ05 and (b) BCFZ15 cathode.

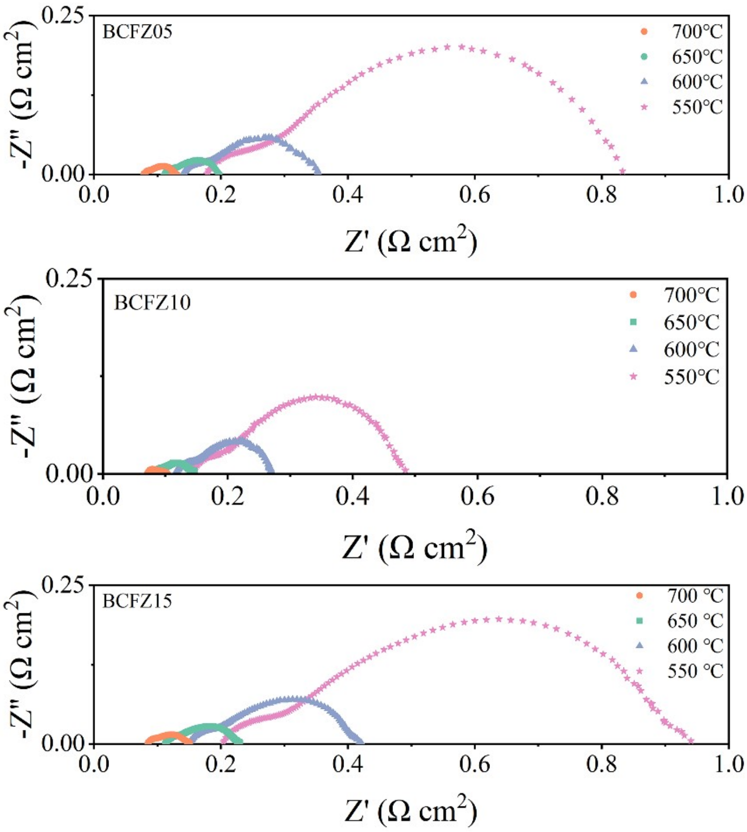

Fig. S8 EIS spectra of the single cell with (a) BCFZ05, (b) BCFZ10 and (c) BCFZ15 cathode exposed to flowing air at 550-700°C.

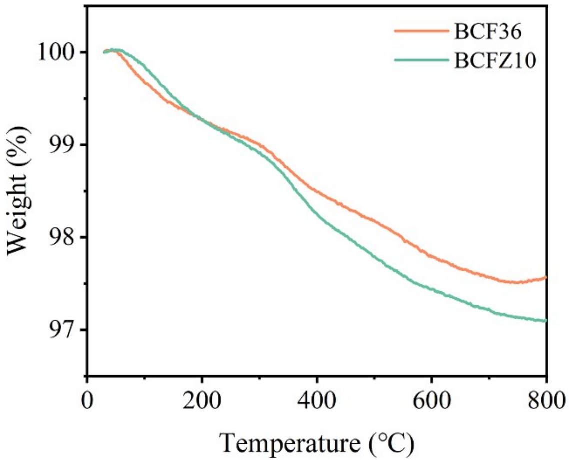

Fig. S9 Thermos gravimetric analysis of BCF36 and BCFZ10 powders.

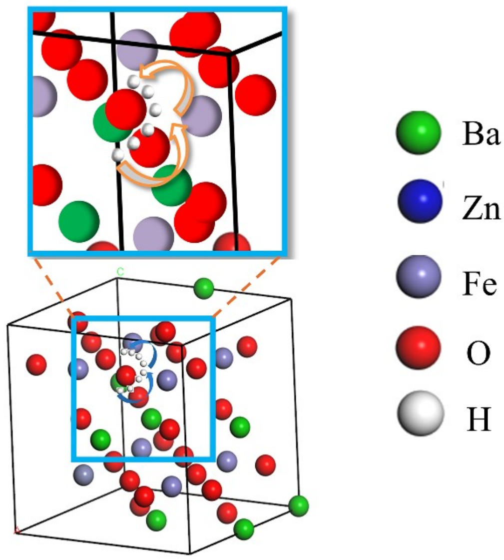

Fig. S10 Simulation schematic of proton migration process.

3. Supplementary Tables

Table. S1 Summary of Rietveld refinements results for BCFZ05, BCFZ10 and BCFZ15 samples.

Sample	Crystal parameters		Phase proportions (wt. %)	Refinement parameters
	Phase structure	crystal axis (Å)		
BCFZ05	Cubic (P m -3 m)	a=b=c=4.0968	72.6	Rw=3.84%, GOF=1.38
	Orthorhombic (P m c n)	a=8.7739 b=6.2029 ,c=6.1996	27.4	
BCFZ10	Cubic (P m -3 m)	a=b=c=4.1103	76.0	Rw=5.09% GOF=1.67
	Orthorhombic (P m c n)	a=8.7643 b=6.2377 c=6.2224	24.0	
BCFZ15	Cubic (P m -3 m)	a=b=c=4.1345	78.3	Rw=4.85%, GOF=1.59
	Orthorhombic (P m c n)	a=8.7650 b=6.2410, c=6.2262	21.7	

Table. S2 Peak deconvolution results of O 1s XPS spectra for BCFZ05, BCFZ10 and BCFZ15 cathode.

Cathode	Binding energy (eV)				O_{ads}/O_{lat}
	Lattice O	O^{2-}/O^{-}	Surface OH^{-}/O^{2-}	Surface H_2O	
BCFZ05	528.17	529.11	530.85	531.57	4.66
BCFZ10	528.22	529.12	530.92	531.54	5.30
BCFZ15	528.52	529.49	531.06	531.57	3.83

Table. S3 The kinetic characteristics of BCFZ10 measured at 550°C-700°C.

Cathode	BCFZ05	BCFZ10	BCFZ15	BCFZ10		
T (°C)		700		650	600	550
D_{ef} (cm^2 S^{-1})	6.7e-4	7e-4	6.65e-4	5e-4	2e-4	7e-5
K_{ef} (cm^2 S^{-1})	1.08e-3	1.15e-3	1.04e-3	6.8e-4	3e-4	1.13e-4

Table. S4 Performance comparison of H-SOFCs using cobalt-free single-phase cathodes reported in the literature and the present study. The performances of these cells were measured at 600°C.

Reference	Cathode	Electrolyte	PPD ($mW\ cm^{-2}$)	Rp ($\Omega\ cm^2$)
[3]	BLFZY	BZCY	305	0.48
[4]	BCFB02	BZCY	371	0.265
[5]	BLF	BZCYY	610	0.211
[6]	BCF36	BZCY	450	0.28
[7]	BCF	SDC	212	0.186
[8]	D-BCF30	BZCYY	711	0.238
[9]	BCYF2	BZCYY	656	0.27
[10]	BFCY-BCFY	BZCY	417	0.25
[11]	BLFZ–BZCYY	BZCYY	142.8	0.683
[12]	BCF-30Pr	BZCY	663	0.152
[13]	C-LSMN7373	BZCYY	386	0.43
[14]	LCNO	BZCY	236	0.491
[15]	PNOF	BZCYY	390	0.49
[16]	SFO2	BZCY	369.2	0.521
[17]	PBKFZ	BZCY	740	0.19
[18]	LSNC	BZCY	858	0.203
this work	BCFZ10	BZCYY	998.6	0.151

Notes：

BZCY = $BaZr_{0.1}Ce_{0.7}Y_{0.2}O_{3-\delta}$

BZCYY = $BaZr_{0.1}Ce_{0.7}Y_{0.1}Yb_{0.1}O_{3-\delta}$

BCFB02 = $BaCe_{0.5}Fe_{0.3}Bi_{0.2}O_{3-\delta}$

BLFZY = $Ba_{0.95}La_{0.05}Fe_{0.8}Zr_{0.1}Y_{0.1}O_{3-\delta}$

BLF=$Ba_{0.95}La_{0.05}FeO_{3-\delta}$

BCF36 = $BaCe_{0.36}Fe_{0.64}O_{3-\delta}$

BCF = $BaCe_{0.05}Fe_{0.95}O_{3-\delta}$

D-BCF30 = $Ba_{0.95}Ce_{0.3}Fe_{0.7}O_{3-\delta}$

BCYF2 = $BaCe_{0.16}Y_{0.04}Fe_{0.8}O_{3-\delta}$

BCFY = $BaCe_{0.7}Fe_{0.1}Y_{0.2}O_{3-\delta}$;

BFCY = $BaFe_{0.8}Ce_{0.1}Y_{0.1}O_{3-\delta}$

BLFZ = $Ba_{0.95}La_{0.05}Fe_{0.8}Zn_{0.2}O_{3-\delta}$

BCF-30Pr = 30wt%Pr_6O_{11}-70wt%$BaCe_{0.2}Fe_{0.8}O_{3-\delta}$

C-LSM73 = Cubic-type $La_{0.7}Sr_{0.3}MnO_{2.95}$

LCNO = $La_{1.5}Ca_{0.5}NiO_{4+d}$

PNOF = $Pr_2NiO_{3.9+\delta}F_{0.1}$–40 wt% BZCYY

SFO2 = $Sr_3Fe_2O_7$–5 wt% BZCY

PBKFZ = $PrBa_{0.9}K_{0.1}Fe_{1.9}Zn_{0.15+\delta}$

LSNC = $La_{1.2}Sr_{0.8}Ni_{0.5}Cu_{0.5}O_{4+\delta}$

BCFZ10 = $BaCe_{0.26}Fe_{0.64}Zn_{0.1}O_{3-\delta}$

Table. S5 Summary of ohmic, polarization and total resistance values of anode-supported single cells with BCFZ05, BCFZ10 and BCFZ15 cathode at 550°C -700°C.

T (°C)	Ro (Ω cm^2)			Rp (Ω cm^2)			Total resistance (Ω cm^2)		
	BCFZ05	BCFZ10	BCFZ15	BCFZ05	BCFZ10	BCFZ15	BCFZ05	BCFZ10	BCFZ15
550	0.178	0.143	0.204	0.655	0.341	0.737	0.833	0.484	0.941
600	0.140	0.117	0.150	0.213	0.151	0.271	0.353	0.268	0.421
650	0.112	0.084	0.112	0.083	0.064	0.116	0.195	0.148	0.228
700	0.079	0.071	0.085	0.049	0.032	0.065	0.128	0.103	0.150

4. Supplementary References

1 Y. Song, Y. Chen, W. Wang, C. Zhou, Y. Zhong, G. Yang, W. Zhou, M. Liu and Z. Shao, *Joule*, 2019, **3**, 2842–2853.

2 L. Zhang, Y. Yin, Y. Xu, S. Yu and L. Bi, *Sci. China Mater.*, 2022, **65**, 1485–1494.

3 Y. Xia, Z. Jin, H. Wang, Z. Gong, H. Lv, R. Peng, W. Liu and L. Bi, *J. Mater. Chem. A*, 2019, **7**, 16136–16148.

4 Y. Wu, J. Hou, Z. Gong, L. Miao, H. Tang and W. Liu, *Journal of Alloys and Compounds*, 2019, **790**, 551–557.

5 F. Dong, D. Chen, Y. Chen, Q. Zhao and Z. Shao, *J. Mater. Chem.*, 2012, **22**, 15071–15079.

6 H. Tong, M. Fu, Y. Yang, F. Chen and Z. Tao, *Adv Funct Materials*, 2022, **32**, 2209695.

7 H. Liu, K. Zhu, Y. Liu, W. Li, L. Cai, X. Zhu, M. Cheng and W. Yang, *Electrochimica Acta*, 2018, **279**, 224–230.

8 Q. Wang, M. Zhang, L. Fan and Z. Tao, *Ceramics International*, 2024, **50**, 14631–14636.

9 D. Zou, Y. Yi, Y. Song, D. Guan, M. Xu, R. Ran, W. Wang, W. Zhou and Z. Shao, *J. Mater. Chem. A*, 2022, **10**, 5381–5390.

10 Z. Wei, J. Wang, X. Yu, Z. Li, Y. Zhao and J. Chai, *International Journal of Hydrogen Energy*, 2021, **46**, 23868–23878.

11 Z. Wang, P. Lv, L. Yang, R. Guan, J. Jiang, F. Jin and T. He, *Ceramics International*, 2020, **46**, 18216–18223.

12 X. Lu, Z. Yang, J. Zhang, X. Zhao, J. Chen, W. Liu, Y. Zhao and Y. Li, *Journal of Power Sources*, 2024, **599**, 234233.

13 N. Wang, S. Hinokuma, T. Ina, C. Zhu, H. Habazaki and Y. Aoki, *J. Mater. Chem. A*, 2020, **8**, 11043–11055.

14 C.-Y. Gu, X.-S. Wu, J.-F. Cao, J. Hou, L.-N. Miao, Y.-P. Xia, Chao-Fu and W. Liu, *International Journal of Hydrogen Energy*, 2020, **45**, 23422–23432.

15 G. Li, Y. Gou, R. Ren, C. Xu, J. Qiao, W. Sun, Z. Wang and K. Sun, *Journal of Power Sources*, 2021, **508**, 230343.

16 K. Dong, J. Hou, L. Miao, Z. Jin, D. Wang, Y. Teng and W. Liu, *Ceramics International*, 2020, **46**, 19335–19342.

17 B. Liu, Z. Li, X. Yang, D. Yan, J. Li and L. Jia, *J. Mater. Chem. A*, 2022, **10**, 17425–17433.

18 C. Jin, L. Ma, J. Gong, W. Liu and J. Hou, *Ceramics International*, 2023, **49**, 35830–35836.